POWER SMOOTHENING OF GRID INTERF ACED DFIG BASED VARIABLE SPEED WIND ENERGY CONVERSION SYSTEM

M Parthasarathi[1], Dr.K Jithender Gowd[2]
[1] PG Scholar, Dept.of Electrical Engineering, JNTUA College of Engineering, Ananatapur, Andhra Pradesh, India.
[2] Assistant Professor, Dept.of Electrical Engineering, JNTUA College of Engineering, Ananatapur, Andhra Pradesh, India.

Abstract: ***This paper presents the analysis, control and design of grid connected DFIG based WECS for power smoothening with maximum power point tracking scheme. In this rotor position is estimated through the sensor less control using rotor position computation algorithm. Unpredictable nature of the wind causes power fluctuations that can be controlled by introducing battery energy storage system in the DC-link between the back to back connected voltage source converters. In this system BESS is presented to supply regulated power to the grid irrespective of wind speed. The control algorithm of grid side converter is modified for feeding regulated power to the grid. Rotor side converter is controlled for achieving MPPT and unity power factor at the stator terminal. This developed DFIG is tested for different wind speeds and steady state and dynamic performance test results are presented for both the PI controller and fuzzy controller.***

Index Terms—Doubly Fed Induction Generator (DFIG), Battery Energy Storage System (BESS), Wind Energy Conversion System (WECS), Maximum Power Point Tracking (MPPT), Sensor less, Power Leveling.

I. INTRODUCTION

Earth's fossil fuel energy resources such as oil, gas and coal are limited in production and are expected to use beyond their peak in the next years, then the price of energy may continue to increase. Continually rising need of the energy in the future can be met by contributing more renewable energy sources. Renewable sources are climate-friendly because of the nonexistence of harmful emissions to the environment [1]. From all renewable energy technologies, the wind energy is one of the lowest-priced because of improvement in power electronic controllers [2].Fixed speed WECSs (Wind Energy Conversion Systems) using squirrel cage induction generators are most commonly used because of their ease and low cost. From the wind turbine characteristics, one can clearly observe that for different wind speeds, the machine should run at different rotor speeds for getting maximum power. As fixed speed induction generators are running at same speed for different wind speeds, fixed speed induction generators (FSIG) are less efficient [3]. In FSIG the stator is directly connected to the grid, these fixed speed generators draw large lagging reactive power. Present days, variable speed induction generators are being used to run at desired speed using power electronic converters to improve the energy output substantially and also to achieve unity power factor [4]. DFIG (Doubly Fed Induction Generator) is the mostly preferred variable speed WECS topology due to the reduction in the size of the power converters and also the converter losses [5-7]. DFIG with single-stage gearbox seems the mainly interesting choice due to its energy yield divided by cost [7]. Vector control techniques have been used to control active and reactive powers of DFIG independently [8-9]. Hybrid energy storage systems connected to wind turbines to analyze the power quality [11].for different time scales, different energy storage technologies are compared on the basis of operational suitability. The suitable sizing of storage and energy capacity required for specific power rating [12]. Fast wind induced power variations are eliminated by introducing super capacitors [13-15]. The voltage fluctuations and power smoothening are achieved by integrating flywheel with DFIG. Continuously increases the wind energy penetration in the grid [16-17]. Flywheel storage is normally preferable for the time scale of 20 minutes [10]. Rapid improvements in Battery Energy Storage System (BESS) have totally changed its applications in high power ratings [18]. Nowadays researchers have started introducing BESS in the WECS for reducing the power variations [19-23]. In [19-20], authors have used separate inverter for the combination of BESS. BESS is also integrated with STATCOM for improving transient stability and also to control the power output [21]. The same functionalities can be achieved by integrating BESS at the DC-link of DFIG. By reducing one converter and the system becomes simple and efficient. Rotor position can be estimated by the rotor position computation algorithm [24]. The uniqueness of the work lies in the control of GSC (Grid Side Converter). The choosing of BESS is the other important aspect of DFIG based WECS for power smoothening.

II. SYSTEM MODELING AND CONTROL PRINCIPLE

DFIG and WCS interface is shown in fig.1 BESS is connected to DC-link in between back to back two voltage source converters. Stator side converter connected to 3-phase grid and rotor side converter is connected to the wind turbine. RSC is controlled by using voltage reference frame. Here synchronously rotating reference frame is used along with the EPLL (Enhanced Phase Locked Loops). Rotor position can be estimated with the help of computational algorithm that can be done at rotor side. Regulated power fed to the grid by controlling the grid side converter and remaining power is stored in BESS. If power produced with wind is less then regulated power the BESS supply the remaining power to the grid that is shown in fig.2.

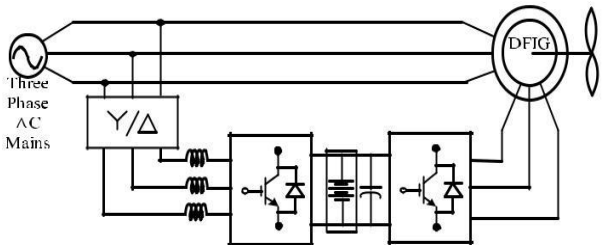

Fig.1 Proposed system configuration.

III. DESIGNING OF VARIABLE SPEED WECS

BESS rating, voltage of BESS and converter ratings selection are much important for the successful operation of WECS. If the BESS rating is high then the system is reliable but the cost is much high. BESS selection is very critical in the economical aspect. The rating of battery voltage and the suitable ratings of the system is listed in appendix.

A .Selection of battery voltage

In general DC-link voltage of the VSC should be greater than twice the peak of phase voltage [25]. Battery voltage is selected by considering the voltages at both GSC and RSC. DFIG operating speed range for WECS is in between 0.7p.u to 1.3p. u. thus the maximum operating slip is 0.3. The maximum RMS phase voltage of the rotor (V_r) is given as,

$$V_r = S_{max} V_p \left(\frac{N_r}{N_s}\right) \quad (1)$$

Where, stator phase voltage V_p = 230V, S_{max} =0.3,
Nr/Ns = rotor to stator turns ratio=1/2.

By substituting the above values, we get rotor phase voltage (V_r) as 34.64V. Star delta transformers is used between GSC and grid with 2:1 turns ratio. So, that phase voltage at GSC (V_{GSC}) = 66.67V. V_{GSC} is more than V_r, so the DC-link voltage should be selected based on V_{GSC}. The DC -link voltage is estimated as,

$$V_{dc} \geq (2\sqrt{2}/m)\, V_{GSC} \quad (2)$$

Maximum modulation index of VSC is chosen as 1 for linear region. So the value of V_{dc} by (2) is 188.57 V. By considering the battery voltage for the minimum state of charge (SOC), and also considering the availability of the battery in the system, the nominal battery voltage is selected as 240 V.

B. Design of Battery Energy Storage System (BESS)

If the size of the battery is large it increases the reliability but initial investment is more. If the rating of the battery is small it affects the reliability. So that for satisfactory operation of the WECS appropriate BESS is necessary. By considering wind profile at the site the storage capacity of BESS is selected. The average power is chosen from particular wind site from past wind data. The excess power stored in to the BESS when the generated power from the DFIG is more than regulated power. Energy is taken from the battery when power generated less than regulated power. The wind speed at turbine height is calculated by using formula [23],

$$\frac{V}{V_0} = \left(\frac{h}{h_0}\right)^n \quad (3)$$

Where, V is the new wind speed at a height h, V_0 is the old wind speed at a height of h_0 and n is terrain factor. Here a terrain factor of 0.13 is selected for the wind speed calibration. The average power may be calculated by considering every day or a month. The rating of the battery bank is

$$E_b = \sum_{i=1}^{n} (P_{mi} * t_i) \quad (4)$$

where, P_{mi} = excess power stored into the battery at every instant and t_i is the time period chosen as 5 minutes in this case. P_{mi} is calculated as,

$$P_{mi} = P_{inst} - P_{avg} \quad (5)$$

Where P_{inst} = instantaneous power at any instant and P_{avg}= average power fed to the grid.

C. Selection of voltage source converter rating

The power flows are different in RSC and GSC because of BESS in the DC-link. When the wind turbine is in shut down condition the maximum power flows through the GSC and the BESS is feeding the total power to the grid. This constant power generation is normally chosen as average power which is 3.85kW in this case. Therefore, the GSC rating is selected as 3.85kVA. RSC rating depends upon the reactive power supplied from the rotor side to get unity power factor at the stator side and also the rotor active power. The DFIG draws a lagging volt ampere reactive (VAR) for its excitation to build the rated air gap voltage. It is calculated from the machine parameters that the lagging VAR of 2kVAR is needed when it is running as a motor. In DFIG case, the operating speed range is 0.7p.u. to 1.3p.u. So the maximum slip (S_{max}) is 0.3. For achieving unity power factor at the stator side, reactive power of 600 VAR (S_{max}*Qs = 0.3*2kVAR) is needed from the rotor side (Q_{rmax}). Maximum rotor active power is S_{max}*P. The power rating of the DFIG is 5 kW. Therefore, the maximum rotor active power (P_{rmax}) is 1.5kW (0.3*5 kW=1.5 kW). So the rating of the VSC used as RSC, S_{rated} is estimated as,

$$S_{rated} = \sqrt{P_{r\,max}{}^2 + Q_{r\,max}{}^2} \quad (6)$$

Thus kVA rating of RSC, S_{rated} is calculated as 1.615 kVA.

IV. CONTROL STRATEGY

GSC, RSC and sensor less operation of DFIG control algorithms are explained in this section. The control of GSC and RSC is shown in schematic diagram presented in fig. 2.

A. RSC control

Both the active and reactive power independent control is achieved by the RSC. By RSC control maximum power point is achieved. It is controlled in voltage oriented reference frame. By controlling the d and q axis reference currents active and reactive powers are controlled respectively. Here PI (Proportional Integral) speed controller is used to get the direct axis rotor reference current (I_{dr}*), this is obtained by processing speed error in PI controller. Speed error (w_{er}) is the difference between reference and estimated rotor speeds (ω_r* and ω_r).

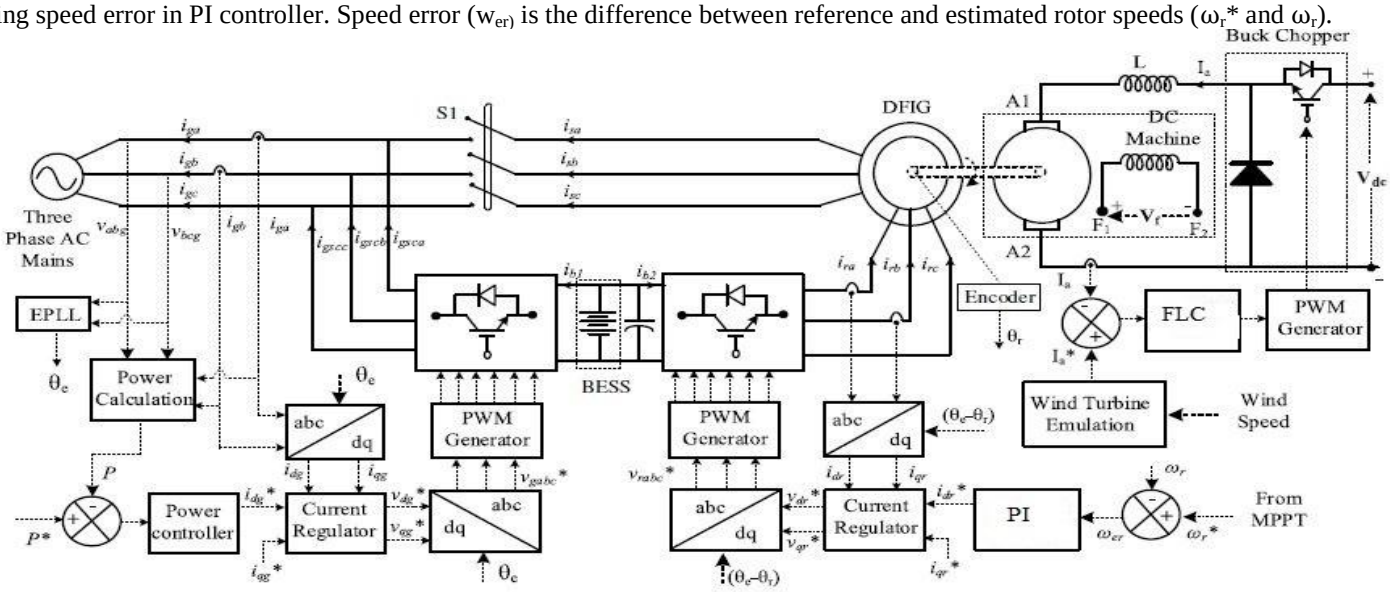

Fig.2 Control algorithm of the proposed WECS.

$$I^*_{dr}(n) = I^*_{dr}(n) + k_{pd}[w_{er}(n) - w_{er}(n-1)] + k_{id}w_{er}(n) \quad (7)$$

Where k_{pd}, k_{id} are the proportional and integral gains of speed proposed. $w_{er}(n)$ and $w_{er}(n-1)$ are the speed errors at n^{th} and $(n-1)^{th}$ instant. I_{dr}*(n) and I_{dr}*(n-1) are the direct axis rotor reference currents at nth and $(n-1)^{th}$ instant.

Using rotor position computation sensor less algorithm the rotor speed (w_r) of DFIG is determined this is discussed in section c.

Reference speed (ω_r*) is chosen for achieving MPPT. The reference rotor speed is estimated using tip speed ratio (TSR) control using wind speed. The reference quadrature axis rotor current (I_{qr}*) is selected to maintain the reactive power to zero at stator terminals. The direct and quadrature axis rotor currents (I_{dr} and I_{qr}) are calculated from sensed rotor currents (i_{ra} ,i_{rb} and i_{rc}) as,

$$I_{dr} = \frac{2}{3}\left[i_{ra}\sin\theta_{slip} + i_{rb}\sin\left(\theta_{slip} - \frac{2\pi}{3}\right) + i_{rc}\sin\left(\theta_{slip} + \frac{2\pi}{3}\right)\right] \quad (8)$$

$$I_{qr} = \frac{2}{3}\left[i_{ra}\cos\theta_{slip} + i_{rb}\cos\left(\theta_{slip} - \frac{2\pi}{3}\right) + i_{rc}\cos\left(\theta_{slip} + \frac{2\pi}{3}\right)\right] \quad (9)$$

Where slip angle (θ_{slip}) is calculated as,

$$\theta_{Slip} = \theta_e - \theta_r \quad (10)$$

The voltage angle θ_e is calculated using EPLL (Enhanced Phase Locked Loop) as shown in Fig. 3. The rotor position θ_r is calculated using RPCA sensorless algorithm as discussed in section C. The direct and quadrature axis currents at the rotor side (I_{dr} and I_{qr}) are controlled close to reference direct and quadrature axis currents (I_{dr}*and I_{qr}*) by using two controllers. The direct and quadrature axis current errors at the rotor side (I_{der} and I_{qer}) are estimated from the actual currents and reference currents of direct and quadrature axis.

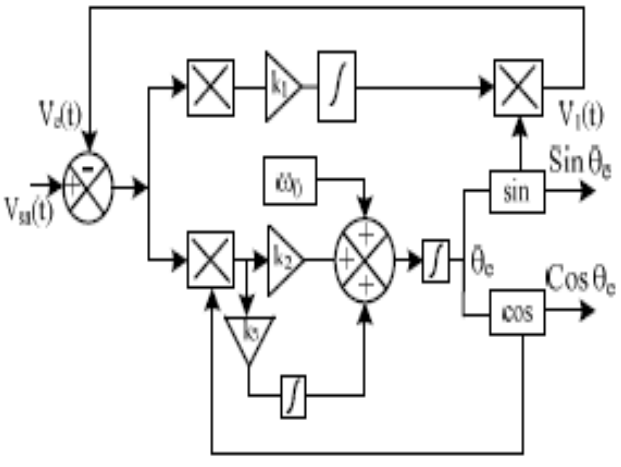

Fig.3. Enhanced Phase Locked Loop (EPLL).

Rotor currents are processed through the PI controller to obtain rotor voltages (V^1_{dr} and V^1_{qr}).

$$V^1_{dr}(n) = V^1_{dr}(n-1) + k_{pdv}\{I_{der}(n) - I_{der}(n-1)\} + k_{idv}I_{der}(n) \quad (11)$$

$$V^1_{qr}(n) = V^1_{qr}(n-1) + k_{pqv}\{I_{der}(n) - I_{qer}(n-1)\} + k_{iqv}I_{qer}(n) \quad (12)$$

Where k_{pdv}, k_{idv} are the proportional and integral gains of direct axis current projected. k_{pqv}, k_{iqv} are the proportional and integral gains of quadrature axis current projected. I_{der} (n) and I_{der} (n-1) are the direct axis current errors at n^{th} and $(n-1)^{th}$ instant. V^1_{dr} (n) and V^1_{dr} (n-1) are direct axis rotor voltages at n^{th} and $(n-1)^{th}$ instant. I_{qer} (n) and I_{qer} (n-1) are the quadrature axis rotor current errors at n^{th} and $(n-1)^{th}$ instant. V^1_{qr} (n) and V^1_{qr} (n-1) are quadrature axis rotor voltages at n^{th} and $(n-1)^{th}$ instant. Direct and quadrature axis rotor voltages (V^1_{dr} and V^1_{qr}) are added with the compensation terms for achieving reference rotor voltages (V_{dr}* and V_{qr}*) as,

$$V_{dr}^* = V_{dr}' - (w_e - w_r)\sigma L_r I_{qr} \quad (13)$$

$$V_{qr}^* = V_{qr}' - (w_e - w_r)(L_m i_{ms} + \sigma L_r I_{dr}) \quad (14)$$

These reference direct and quadrature voltages (V_{dr}*, V_{qr}*) are converted into three phase reference rotor voltages (v_{ra}*,v_{rb}*, v_{rc}*) as,

$$v_{ra}^* = V_{dr}^* \sin\theta_{slip} + V_{qr}^* \cos\theta_{slip} \quad (15)$$

$$v_{rb}^* = V_{dr}^* \sin\left(\theta_{slip} - \frac{2\pi}{3}\right) + V_{qr}^* \cos\left(\theta_{slip} - \frac{2\pi}{3}\right) \quad (16)$$

$$v_{rc}^* = V_{dr}^* \sin\left(\theta_{slip} + \frac{2\pi}{3}\right) + V_{qr}^* \cos\left(\theta_{slip} + \frac{2\pi}{3}\right) \quad (17)$$

These three phase rotor reference voltages (v_{ra}*, v_{rb}*, v_{rc}*) are compared with triangular carrier wave of switching frequency for generating the PWM signals for the Insulated Gate Bipolar Transistors (IGBTs) of the RSC.

B.GSC control

The importance of this work lies in the control of GSC. On the voltage oriented reference frame control of GSC is realized. By controlling the Direct and Quadrature grid currents the real and reactive powers fed to the grid are controlled respectively. Direct axis grid current are determined from reference power (P*).

$$I^*_{dg} = \left(\frac{2}{3}\right)\left(P^*/V_{dg}\right) \quad (18)$$

I^*_{qg} is selected as zero to get unity power factor at AC mains. From the sensed grid currents the actual direct and quadrature grid currents (I_{dg} and I_{qg}) are estimated. The errors in direct and quadrature grid currents (I_{deg} and I_{qeg}) are processed through PI controller as shown as,

$$V^1_{dg}(n) = V^1_{dg}(n) + k_{pdv}\left[I_{deg}(n) - I_{deg}(n-1)\right] + k_{idv}I_{deg}(n) \quad (19)$$

$$V^1_{qg}(n) = V^1_{qg}(n) + k_{pqv}\left[I_{qeg}(n) - I_{qeg}(n-1)\right] + k_{iqv}I_{qeg}(n) \quad (20)$$

Where k_{pdv}, k_{idv} are the proportional and integral gains of direct axis current controller. k_{pqv}, k_{iqv} are proportional and integral gains of quadrature axis current controller. I_{deg} (n) and I_{deg} (n-1) are direct axis current errors at n^{th} and $(n-1)^{th}$ instant. $V_{dg}{}^1$ (n) and $V_{dg}{}^1$ (n-1) are the direct axis grid voltages at n^{th} and $(n-1)^{th}$ instant. I_{qeg} (n) and I_{qeg} (n-1) are the quadrature axis grid current errors at n^{th} and $(n-1)^{th}$ instant. $V_{qg}{}^1$ (n) and $V_{qg}{}^1$ (n-1) are the quadrature axis grid voltages at n^{th} and $(n-1)^{th}$ instant.

Direct and quadrature axis grid voltages ($V_{dg}{}^1$ and $V_{qg}{}^1$) are added with the compensation terms for achieving reference direct and quadrature axis grid voltages (V_{dg}* and V_{qg}*). Three phase reference grid voltages (v_{ga}*, v_{gb}*, v_{gc}*) are calculated from the reference direct and quadrature voltages (V_{dg}*, V_{qg}*).These reference grid voltages (v_{ga}*, v_{gb}*, v_{gc}*) are compared with PWM signals and then these pulses are fed to the GSC.

C. Rotor position computation algorithm

In this algorithm, rotor current (i_r) makes an angle θ_s with the stator co-ordinate system and the rotor current (i_r) makes an angle θ_r with rotor co-ordinate system. The angle between the stator and rotor is calculated as $(\theta_m)_{est} = (\theta_s - \theta_r)$. The schematic diagram of sensor less scheme is shown in fig.4. The rotor currents are transformed from three phase to two phase ($i_{r\alpha}$ and $i_{r\beta}$) by using the Clarke's transformation.

$$\cos\theta_r = \frac{i_{r\alpha}}{\sqrt{i^2_{r\alpha} + i^2_{r\beta}}} \quad (21)$$

$$\sin\theta_r = \frac{i_{r\beta}}{\sqrt{i^2_{r\alpha} + i^2_{r\beta}}} \quad (21)$$

The unit templates of rotor currents aligned to the stator coordinate system ($\cos\theta_s$, $\sin\theta_s$) are calculated as,

$$\cos\theta_s = \frac{i_{rs\alpha}}{\sqrt{i^2_{rs\alpha} + i^2_{rs\beta}}} \quad (23)$$

$$\sin\theta_s = \frac{i_{rs\beta}}{\sqrt{i^2_{rs\alpha} + i^2_{rs\beta}}} \quad (24)$$

Where $i_{rs\alpha}$ and $i_{rs\beta}$ are the rotor currents aligned in stator coordinate system is calculated as,

$$i_{rs\alpha} = \frac{v_{s\beta} - R_s i_{s\beta} - \omega_e L_s i_{s\alpha}}{\omega_e L_m} \quad (25)$$

$$i_{rs\beta} = \frac{v_{s\alpha} - R_s i_{s\alpha} - \omega_e L_s i_{s\beta}}{\omega_e L_m} \quad (26)$$

Stator currents (i_{sa}, i_{sb}), stator voltages (v_{sa}, v_{sb}) are transformed into two phase system using Clarke's transformation ($i_{s\alpha}$, $i_{s\beta}$, vsα and $v_{s\beta}$).The unit vectors of rotor position angle are computed as

$$\text{Cos}\,(\theta_m)_{est} = \cos(\theta_s)\cos(\theta_r) + \sin(\theta_s)\sin(\theta_r) \quad (27)$$

$$\text{Sin}\,(\theta_m)_{est} = \sin(\theta_s)\cos(\theta_r) - \cos(\theta_s)\sin(\theta_r) \quad (28)$$

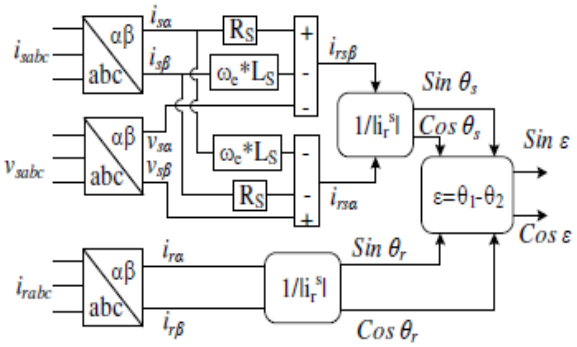

Fig. 4. Rotor Position Computation Algorithm.

V. FUZZY LOGIC CONTROLLER

Fuzzy Logic Controller (FLC) design even though PI controller can play an significant role in stability of the power system and especially for damping of inter area oscillation, the best performance of the PI controller and hence the performance of the DFIG depend on a appropriate choice of the PI gains. Tuning the PI gains to make optimal operation is difficult task, especially, when the process is nonlinear and may change during operation. Fuzzy controller introduces a systematic technique to control a nonlinear procedure based on human experience. The fuzzy controller operation is based on its capability to simulate several role implications at the same time procedure, and the output results are significantly comprehensive. FLC controller is shown in fig.5 and it has Fuzzifier, Inference, Knowledge base and Defuzzifier. FLC has a five membership functions for the error, change in error and the output. The basic fuzzy sets of membership functions for the variables are as shown in the Fig.6a, 6b and 6c. The fuzzy variables are expressed by linguistic variables they are positive large (PB), positive small (PS), zero (ZE), negative small (NS), negative large (NB), for all three variables. The rules are set based upon the knowledge of the system and the working of the system. The rule base adjusts the duty cycle for the PWM of the inverter according to the changes in the input of the FLC. The number of rules can be set as desired. The numbers of rules are 25 for the five membership functions of the error and the change in error (inputs of the FLC) shown below.

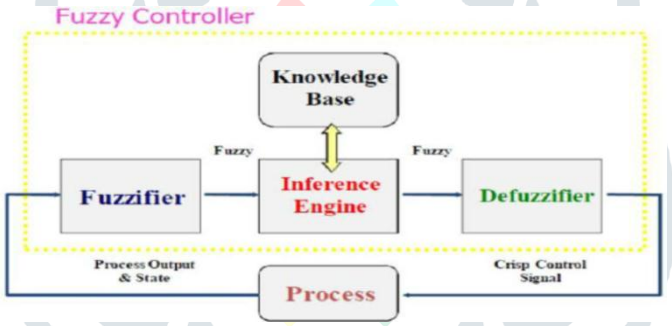

Fig.5. fuzzy logic controller.

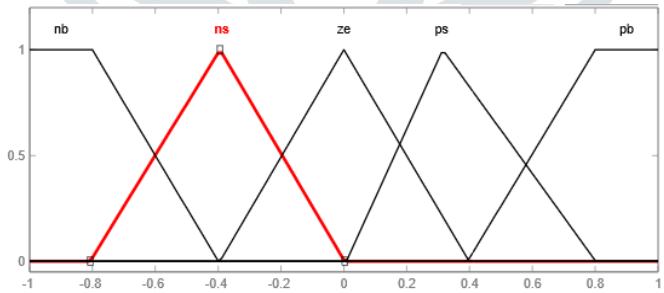

Fig. 6a. membership functions of error.

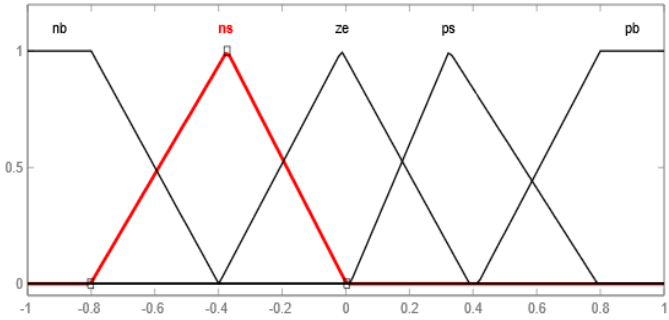

Fig. 6b. membership functions of change in error

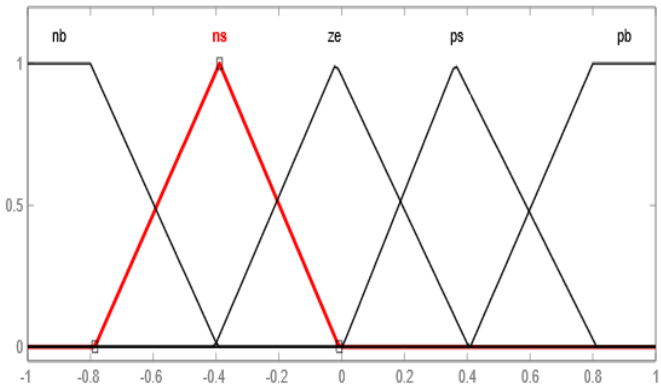

Fig.6c. membership functions of controlled output.

Table2: FLC Rules

$e/\Delta e$	NB	NS	ZE	PS	PB
NB	PB	PB	PB	PB	PB
NS	PB	PB	PS	PS	PB
ZE	ZE	ZE	ZE	PS	PB
PS	NS	NS	NS	NS	PB
PB	NB	NB	NB	NB	PB

VI. SIMULATION RESULTS

The steady state and dynamic behaviors of regulated power DFIG based WECS is presented in this part. Test results are recorded in terms of line voltage (V_{ab}), grid currents (I_{ga}, I_{gb} and I_{gc}), stator currents (I_{sa}, I_{sb} and I_{sc}), GSC currents (I_{gsca}, I_{gscb} and I_{gscc}), rotor currents (I_{ra}, I_{rb} and I_{rc}), stator power (P_S), Grid Power (P_G), GSC power (P_{GSC}), battery voltage (V_b), battery current (I_b), quadrature axis rotor current (I_{qr}), direct axis rotor current (I_{dr}), quadrature axis reference rotor current (I_{qr}*), direct axis reference rotor current (d_r*), rotor speed ($\boldsymbol{\omega}_r$), reference rotor speed ($\boldsymbol{\omega}_r$*) and wind speed (V_w). The power that is discharging from the battery through GSC and RSC are considered as positive.

A. Steady state performance of proposed WECS

Test results are presented for a specific wind speed in all three cases such as sub-synchronous, synchronous and super synchronous speeds as shown in Figs.7-9. In this study, a regulated power is selected as 1.25 kW. So, the grid power is maintained as 1.25 kW irrespective of the wind speed. Fig 7a to 7c at the fixed wind speed of 7m/sec. For getting MPPT from the wind turbine the reference rotor speed is selected as 0.7 p.u. from the fig 7a to 7c we observe that the grid power is maintained at 1.25kw and stator power is 0.902kw due to the low wind speed and the remaining power is coming from the BESS. For the fixed wind speed of 8.5m/sec. For getting MPPT from the wind turbine the reference rotor speed is selected as 0.86 p.u. From the fig 8a to 8c we observe that the grid power is maintained at 1.25kw. Stator power is more than the reference power that is 1.486kw so the excess power stored in to the BESS. For the fixed wind speed of 9.15m/sec. For getting MPPT from the wind turbine the reference rotor speed is selected as 1500rpm from the fig 9a to 9c we observe that the grid power is maintained at 1.25kw. Stator power is more than the reference power that is 2.247kw so the excess power stored in to the BESS .Fig. 10 shows the effective working of sensor less algorithm at different rotor speeds.

B. Dynamic performance of WECS at change in wind speed

Test results are also presented for dynamic changes in wind speed as shown in Figs. 11. Fig. 11 demonstrates the successful operation of proposed DFIG based WECS for the increase in wind speed. With the increase in wind speed, reference rotor speed is increasing for achieving MPPT operation. So the actual rotor speed is increasing because of the speed FLC controller as shown in Fig. 11(a). So the power generation increases from the stator ($P_{S)}$ as shown in Fig. 11(a). The grid power (P_G) is maintained at fixed value. At reduced wind speeds, the stator power is less. So, the battery is discharging through GSC. As the rotor speed increases, stator power increases, so the GSC power is reversed and the battery is charging. As shown in Fig. 11(b), the rotor currents have changed their phase sequence the speed varying from sub-synchronous to super-synchronous speeds. Battery current flowing through GSC and RSC are getting reversed with an increase in the wind speed as shown in Fig. 11(c).

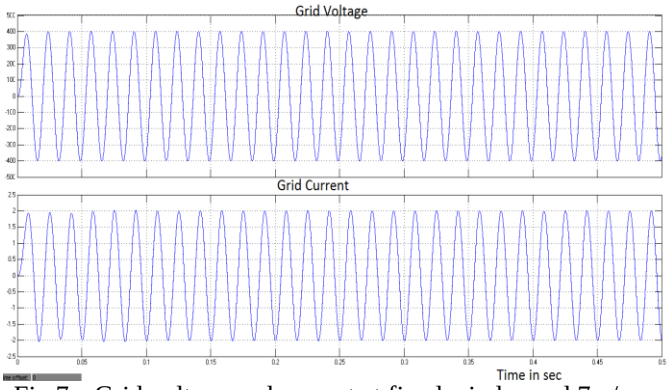

Fig.7a. Grid voltage and current at fixed wind speed 7m/sec.

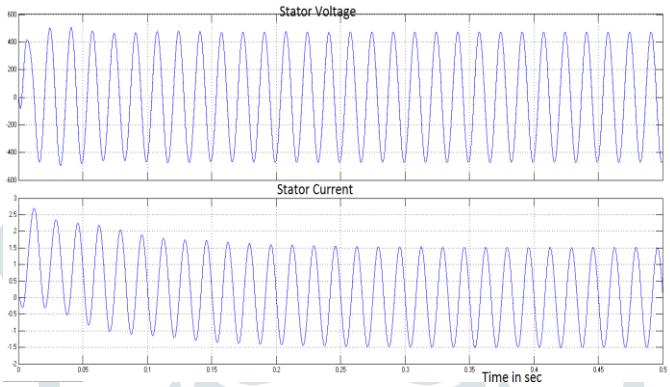

Fig.8b. Stator voltage and current at fixed wind speed 8.5m/sec.

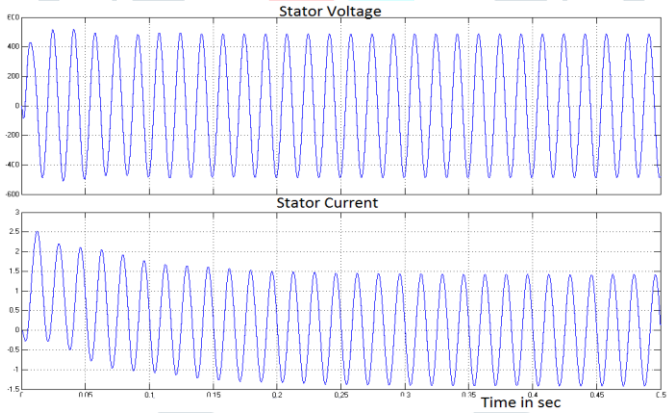

Fig.7b. Stator voltage and current at fixed wind speed 7m/sec.

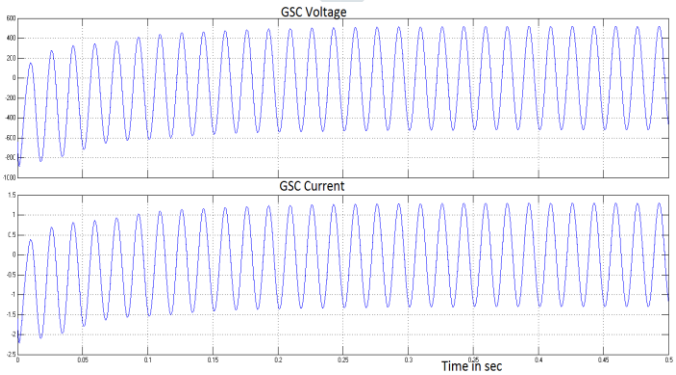

Fig.7c. GSC voltage and current at fixed wind speed 7m/sec.

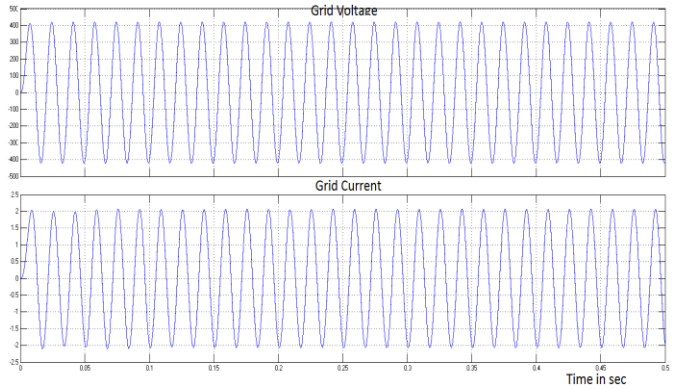

Fig.8a. Grid voltage and current at fixed wind speed 8.5m/sec.

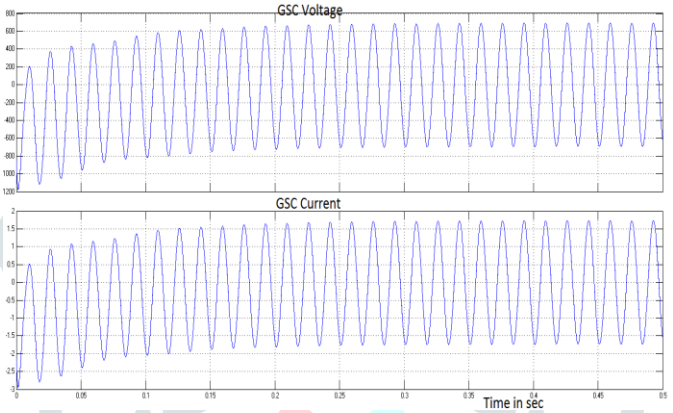

Fig.8c. GSC voltage and current at fixed wind speed 8.5m/sec

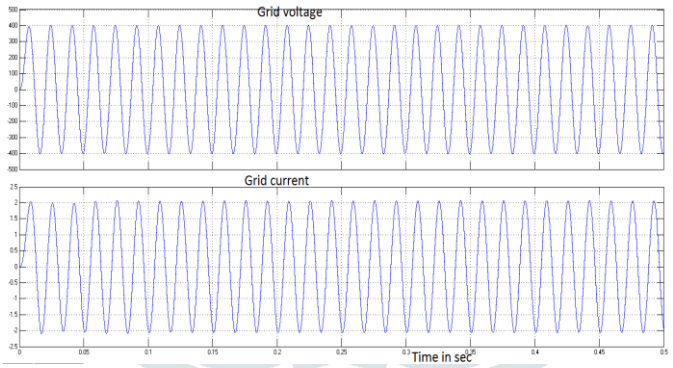

Fig.9a. Grid voltage and current at fixed wind speed 9m/sec

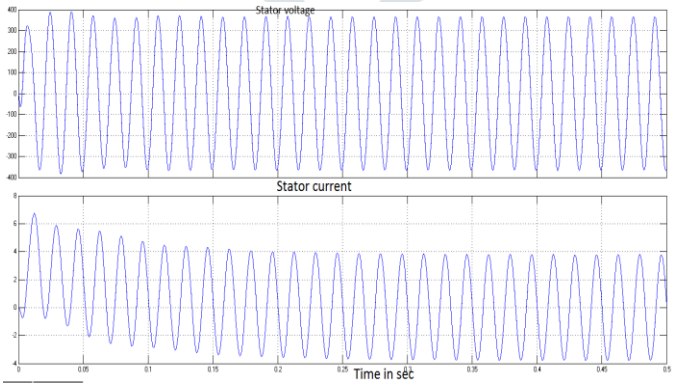

Fig.9b. Stator voltage and current at fixed wind speed 9m/sec.

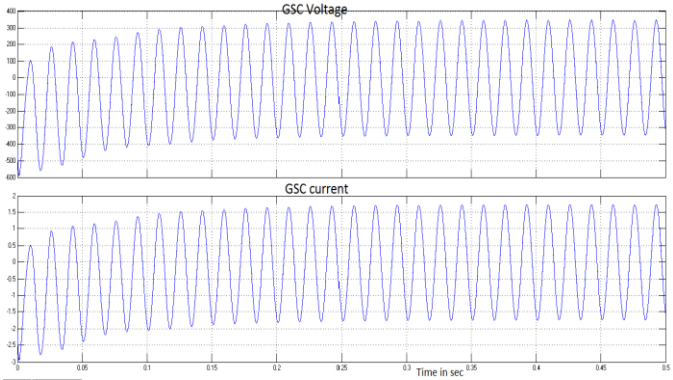

Fig.9c. GSC voltage and current at fixed wind speed 9m/sec.

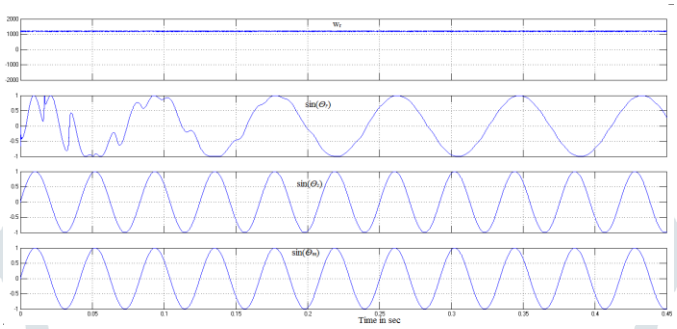

Fig.10 (a)

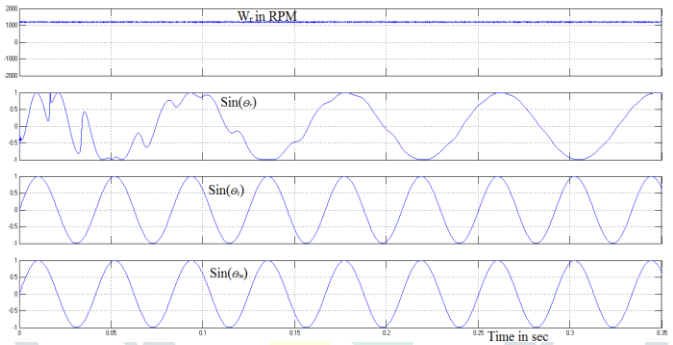

Fig.10 (b)

Fig.10. Steady state performance of the sensor less algorithm of constant power DFIG based WECS at fixed wind speeds (a)-(b) rotor speed (w_r), unit

Templates of rotor currents aligned to rotor axis (sin(Θ_r)), unit templates of rotor currents aligned to stator axis (sin(Θ_s)) and unit vectors of rotor position angle (sin(Θ_m)).

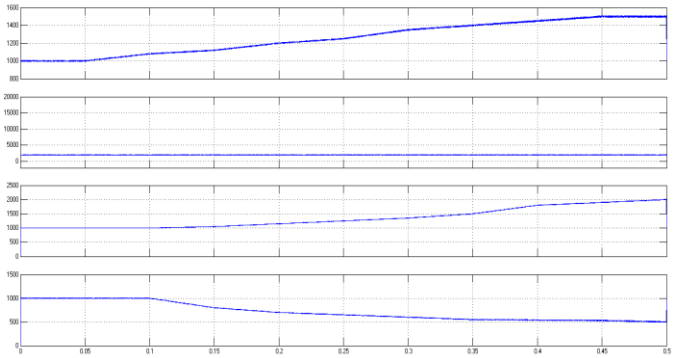

Fig.11. Dynamic performance of proposed DFIG based WECS under rise in wind speed, 11 (a) rotor speed (w_r), grid power (P_G), stator power (Ps) *and* GSC power (P_{GSC}).

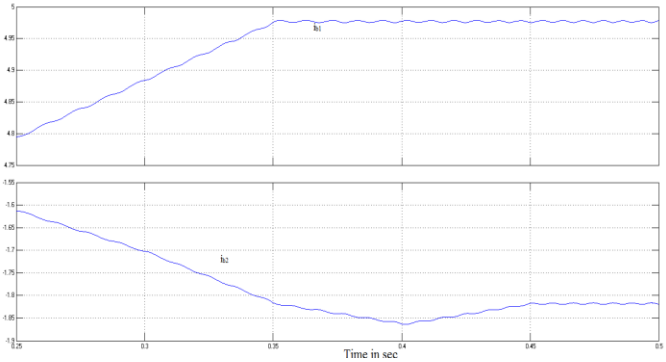

Fig.11 (b).battery current towards GSC(i_{b1}), battery current towards RSC(i_{b2})

THD comparison Table:

FIG.7	**PI**	**FLC**
Grid V&I	19.33	18.26
Source V&I	36.81	24.67
Stator V&I	52.79	23.58

FIG.8	**PI**	**FLC**
Grid V&I	19.33	18.26
Source V&I	36.81	22.61
Stator V&I	52.79	23.58

FIG.9	**PI**	**FLC**
Grid V&I	22.87	18.26
Source V&I	36.81	22.61
Stator V&I	52.79	23.58

FIG.11	**PI**	**FLC**
Rotor current	30.77	24.42

VII. CONCLUSION

In the proposed DFIG based WECS FLC is used to control the RSC. So that the THD is reduced and power quality is improved. The control algorithm for RSC has been implemented for sensorless and to get MPPT. The control algorithm for GSC is designed to feeding regulated power to the grid. This WECS has been found advantageous for supplying regulated power to the grid even under reduced wind speeds and also at high speeds with the help of BESS.

APPENDIX

*A.*WRIM- 3.7kW, R_s=1.32 ohm, L_{ls}=6.832mH, R_2=1.708ohm, L_{lr}=6.832mH, R_c=419.646 ohm, L_m=0.219H, J =0.1878 kg-m^2, stator to rotor turns ratio N_r/N_s=1/2, stator
rated rms current I_s=12 A, rotor rated rms current I_r=18 A.
B. DC Machine- R_a=1.3 ohms, R_f=220 ohms, L_a=7.2mH,
L_f=7.5mH, K_Φ=1.3314.

REFERENCES

[1] Manfred Stiebler, "*Wind Energy Systems for Electric Power Generation*",Springer 2008.

[2] Hermann-Josef Wagner and Jyotirmay Mathur, "*Introduction to Wind Energy Systems Basics, Technology and Operation*", Springer 2009.

[3] S. S. Murthy, B. Singh, P. K. Goel and S. K. Tiwari, "A Comparative Study of Fixed Speed and Variable Speed Wind Energy Conversion Systems Feeding the Grid", *in Proc. IEEE 7th International Conference Power Electronics and Drive Systems, 2007 PEDS '07,* 27-30 Nov. 2007,pp.736-743.

[4] M. Mansour, M. N. Mansouri and M. F. Mimouni, "Comparative study of fixed speed and variable speed wind generator with pitch angle control,"*International Conference on Communications, Computing and Control Applications (CCCA),* 3-5 March 2011, pp. 1-7.

[5] R. Datta and V. T. Ranganathan, "variable-speed wind power generation using doubly fed wound rotor induction machine-a comparison with alternative schemes," *IEEE Trans. Energy Con.,* vol.17, no.3, pp. 414-421, Sep 2002.

[6] L. Holdsworth, X. G. Wu, J. B. Ekanayake and N. Jenkins, "Comparison of fixed speed and doubly-fed induction wind turbines during power system disturbances," IEE *Proc. Generation, Transmission and Distribution,* vol. 150, no. 3, pp. 343-352, 13 May 2003.

[7] H. Polinder, F. F. A. van der Pijl, G. J. de Vilder and P. J.Tavner, "Comparison of direct-drive and geared generator concepts for

wind turbines," *IEEE Trans. Energy Con.,* vol. 21, no. 3, pp.725 -733,May 2005.

[8] S. Muller, M. Deicke and R. W. De Doncker, "Doubly fed induction generator systems for wind turbines," *IEEE Industry Applications Magazine,* vol.8, no.3, pp.26-33, May/Jun 2002.

[9] R. Pena, J. C. Clare and G.M Asher, "Doubly fed induction generator using back-to-back PWM converters and its application to variable-speed wind-energy generation," *Proc. Electric Power Applications,* vol. 143,no. 3, pp. 231 – 241, May 1996.

[10] Changling Luo, H. Banakar, B. Shen and Boon - Teck Ooi, "Strategies to Smooth Wind Power Fluctuations of Wind Turbine Generator," *IEEE Trans. Energy Con.,* vol.22, no.2, pp.341-349, June 2007.

[11] Youngil Kim and R. Harrington, "Analysis of various energy storage systems for variable speed wind turbines," *2015 IEEE Conference on Technologies for Sustainability (SusTech),* Ogden, UT, 2015, pp. 7-14.

[12] J. P. Barton and D. G. Infield, "Energy storage and its use with intermittent renewable energy," *IEEE Transactions on Energy Conversion,* vol.19, no.2, pp. 441-448, June 2004.

[13] C. Abbey and G. Joos, "Super capacitor Energy Storage for Wind Energy Applications," *IEEE Transactions on Industry Applications,* vol. 43, no.3, pp. 769-776, May-June 2007.

[14] Liyan Qu and Wei Qiao, "Constant Power Control of DFIG Wind Turbines With Super capacitor Energy Storage," *IEEE Transactions on Industry Applications,* vol.47, no.1, pp. 359-367, Jan.-Feb. 2011.

[15] G. Mandic, A. Nasiri, E. Ghotbi and E. Muljadi, "Lithium-Ion Capacitor Energy Storage Integrated With Variable Speed Wind Turbines for Power Smoothing," *IEEE Journal of Emerging and Selected Topics in Power Electronics,* vol. 1, no. 4, pp. 287-295, Dec. 2013.

[16] R. Cardenas, R. Pena, G. Asher and J. Clare, "Power smoothing in wind generation systems using a sensorless vector controlled induction Machine driving a flywheel," *IEEE Trans. on Energy Conv.,* vol.19, no.1,pp. 206 - 216, March 2004.

[17] S. Ghosh and S. Kamalasadan, "An Energy Function-Based Optimal Control Strategy for Output Stabilization of Integrated DFIG-Flywheel Energy Storage System," *IEEE Trans. Smart Grid,* vol. no.99, pp. 1-10,2016.

[18] Daniel H. Doughty, Paul C. Butler, Abbas A. Akhil, Nancy H. Clark and John D. Boyes, *"Batteries for Large-Scale Stationary Electrical Energy Storage"* The Electrochemical Society Interface, Fall 2010.

[19] T. Kai and A. Tanaka "A new smooth scheme for power fluctuation using inverter of wind power generation with doubly fed induction generator,"*International Conf. on Electrical Machines and Systems,* 2008, ICEMS 2008, 17-20 Oct. 2008, pp. 2390 - 2395.

[20] S. Rahmani, A. Hamadi, A. Ndtoungou, K. Al-Haddad and H. Y. Kanaan,"Performance evaluation of a PMSG-based variable speed wind generation system using maximum Power Point Tracking," *in Proc. Of IEEE Electrical Power and Energy Conference (EPEC),* 10-12 Oct. 2012,pp. 223-228.

[21] A. Kanchanaharuthai, V. Chankong and K. A. Loparo, "Transient Stability and Voltage Regulation in Multimachine Power Systems Vis-à-Vis STATCOM and Battery Energy Storage," *IEEE Trans. Power Systems,* vol. 30, no. 5, pp. 2404-2416, Sept. 2015.

[22] Y. Mishra, S. Mishra and Li Fangxing, "Coordinated Tuning of DFIGBased Wind Turbines and Batteries Using Bacteria Foraging Technique for Maintaining Constant Grid Power Output," *IEEE Systems Journal,*vol.6, no.1, pp.16-26, March 2012.

[23] V. C. Ganti, B. Singh, S. K. Aggarwal and T. C. Kandpal, "DFIG-Based Wind Power Conversion with Grid Power Leveling for Reduced Gusts,"*IEEE Trans. Sustainable Energy,* vol.3, pp.12-20, Jan. 2012.

[24] A. Karthikeyan, C. Nagamani and G. S. Ilango, "A Versatile Rotor Position Computation Algorithm for the Power Control of a Grid Connected Doubly Fed Induction Generator," *IEEE Trans. Energy Conversion,* vol.27, no.3, pp.697 - 706, Sept. 2012.

[25] S Sharma and B Singh, "Voltage and frequency control of asynchronous generator for stand-alone wind power generation," *IET Power Electronics,* vol.4, no.7, pp.816-826, Aug. 2011.